Visible-light-enhanced photothermocatalytic activity of ABO₃-type perovskites for the decontamination of gaseous styrene

Jiangyao Chen [a,b], Zhigui He [a,e], Guiying Li [b], Taicheng An [a,b,*], Huixian Shi [c], Yuanzhi Li [d]

[a] State Key Laboratory of Organic Geochemistry and Guangdong Provincial Key Laboratory of Environmental Protection and Resources Utilization, Guangzhou Institute of Geochemistry, Chinese Academy of Sciences, Guangzhou 510640, China
[b] Guangzhou Key Laboratory of Environmental Catalysis and Pollution Control, School of Environmental Science and Engineering, Institute of Environmental Health and Pollution Control, Guangdong University of Technology, Guangzhou 510006, China
[c] School of Materials Science and Engineering, Taiyuan University of Technology, Taiyuan 030024, China
[d] State Key Laboratory of Silicate Materials for Architectures, Wuhan University of Technology, Wuhan 430070, China
[e] University of Chinese Academy of Sciences, Beijing 100049, China

ABSTRACT

ABO₃-type perovskites (A = La, Ce, Sm; B = Cr, Mn, Fe, Co, Ni) were systematically fabricated via a facile soft-templated sol-gel with post-calcination method through a complexation-carbonation-oxidation process, which were successfully applied in the visible-light-driven photothermocatalytic degradation of volatile organic compounds (VOCs) for the first time. Preliminary characterization results revealed the lower impact to the oxidative performance and visible-light-absorption properties of ANiO₃ than LaBO₃, while the latter ones should present more attractive promotion of catalytic performance toward VOC degradation. Subsequently catalytic degradation of VOCs using gaseous styrene as model compound confirmed that all LaBO₃-type perovskites possessed both high visible-light-driven photocatalytic and temperature-induced thermocatalytic activities. Meanwhile, synergetic effect between photocatalysis and thermocatalysis activities of different position B substituted LaBO₃ resulted in different enhancement of their photothermocatalytic activities, where the highest synergistic factor (3.53) was obtained for LaMnO₃ at 140 °C. Besides, the synergetic effect could also effectively preserve the activity of the perovskite catalysts (eg. LaMnO₃) that almost the same removal efficiency (ca. 96.6% within 40 min) was obtained to styrene (initial concentration of 40 ppmv) after five continuous cycling tests. The highly and stably photothermocatalytic activity of these perovskites were attributed to the coefficient effect of the small crystal size and narrower bandgap as well as high visible light absorption and reducibility. This work could provide an efficient and practical way to utilize the total energy of sun for the remediation of atmospheric environment pollutions.

© 2017 Elsevier B.V. All rights reserved.

1. Introduction

As a derivative of benzene and one of typical volatile organic compounds (VOCs), styrene is an indispensable monomer for the industrial manufacture of resin, rubber, etc. Unfortunately, during the application and post-application stages of these synthetic materials [1,2], styrene will inevitably emit into atmosphere and cause serious neurotoxic, hematological, cytogenetic and carcinogenic effects on humans after long-term continuous exposure [3]. Therefore, the removal of VOCs such as styrene is urgent for environment and human health protection.

Among the developed technologies, thermocatalysis has been widely applied owing to its more economic feasibility and effectiveness for VOC abatement [4]. Of this technology, catalyst plays a very decisive role in the high pollutant elimination efficiency, which generally includes two groups: noble metals and metal oxides. In comparison with noble metals, metal oxides have been regarded as more promising catalysts due to the advantages of less inexpensive and comparatively high activity [5]. Recently, perovskite-type metal oxides with general formula ABO₃ have been found to be effective catalysts for the total oxidation of VOCs. For example, Jung et al. reported 100% of thermocatalytic efficiency toward

gaseous benzene and toluene on $LaCoO_3$ and $LaMnO_3$ at 360 °C and 310 °C, respectively [6,7]. Zhang et al. also revealed the complete thermocatalytic mineralization of gaseous toluene on $LaMnO_3$ [8]. Nevertheless, much high energy (temperature > 200 °C) is needed to achieve complete removal of VOCs for the reported perovskites [9,10]. In fact, by combining the thermocatalysis with photocatalysis, much lower temperature with even higher activity were observed for a series of metal oxides such as CeO_2 [11], TiO_2 [12,13], MnO_x [14] and their composites [15,16] toward VOC degradation. This is due to that the introduction of light into thermocatalysis system could efficiently promote synergetic photothermal effect, resulting in more electron excitation, relaxation, intensified heat emission and then enhanced photothermocatalytic activity. Thus, the combination of thermocatalysis and photocatalysis in perovskite system might also be beneficial for further enhancement of their catalytic ability to VOCs, while the premise is that perovskite must also be a good photocatalyst candidate.

Luckily, perovskites have shown excellent promising as efficient visible-light-driven photocatalysts, ascribing to their advantages of favorable band edge potentials, altered band structure and other photophysical properties [17,18]. Previous reports have also confirmed their high visible light photocatalytic degradation activity toward aqueous contaminants such as dyes [19,20] and phenol [21]. But rare application in the photocatalytic purification of gaseous pollutants on perovskites has been reported yet [22,23], not to say their visible-light-driven photothermocatalytic utilizations. Moreover, the contribution of visible light to the synergetic effect of photocatalysis and thermocatalysis, and then enhancement of photothermocatalytic activity and stability toward VOCs on the perovskites is still unknown. Actually, taking the advantages of both photocatalysis and thermocatalysis of perovskites, photothermocatalysis technique should be a novel strategy for the efficient abatement of VOCs at low temperature range, since it could utilize renewable solar energy and avoid the disadvantages of single technique.

Therefore, in this study, a series of visible-light-responded ABO_3 (A = La, Ce, Sm; B = Cr, Mn, Fe, Co, Ni) perovskites have been synthesized via a facile sol-gel with post-calcination method using polyethylene glycol as the soft template. The structural, morphological, optical and oxidation properties of the prepared perovskites were investigated detailed. Meanwhile, the possible formation mechanism was tentatively proposed based on the characteristic results. Finally, the photocatalytic, thermocatalytic and photothermocatalytic activities of the prepared perovskites were comparably evaluated by the degradation of typical VOCs, i.e., styrene, under visible light illumination or(/and) different temperatures to reveal the synergetic mechanism of photocatalysis with thermocatalysis to the enhancement of photothermocatalytic activity toward styrene degradation.

2. Experimental

2.1. Synthesis

A simple soft-templated sol-gel with post-calcination method was applied for the synthesis of ABO_3 (A = La, Ce, Sm; B = Cr, Mn, Fe, Co, Ni) perovskites. Typically, 6 g of polyethylene glycol (PEG, M = 600), 5 mM of $La(NO_3)_3 \cdot 6H_2O$, 5 mM of $Mn(NO_3)_2$ and 28 mL of citric acid solution (0.4 M) were mixed at room temperature under stirring for 1 h. Then, the mixture was continuously stirred at 80 °C until sol was formed, then was transferred into a vacuum tube furnace and dried at 90 °C for 12 h under N_2 atmosphere to obtain gel. Finally, the ABO_3 perovskites were obtained after calcined at 700 °C for 2 h.

2.2. Characterization

X-ray diffraction (XRD) data was obtained by using a Rigaku Dmax 2200 V X-ray diffractometer. The oxidation property of the prepared samples was investigated on a TP-5078 multifunction adsorption instrument. The UV–vis absorption spectra (UV–vis) were measured with a UV-2501PC UV–vis spectrophotometer. Images were obtained on a scanning electron microscopy (SEM, JSM-6330F). The thermal process of the as-prepared sample was heated from 100 °C to 1000 °C with a heating rate of 5 °C min^{-1} at a flow rate of 40 mL min^{-1} in O_2 atmosphere with TG/DSC (Netzsch STA 449F3). Fourier transform-infrared (FT-IR) spectroscopy analysis of the perovskites was performed using FT-IR colet/Nexus 670 spectrophotometer.

2.3. Catalytic performance evaluation

The photocatalytic (PC), thermocatalytic (TC) and photothermocatalytic (PTC) performances of the prepared samples were measured in a stainless steel cylinder reactor with the volume of 5.56 L as shown in Fig. S1. During the experiment, a given amount of liquid styrene was injected into the reactor and reached equilibrium with the assist of a micro-circulation pump, and the final concentration of gaseous styrene was about 40 ppmv. After that, the catalytic experiments started when *ca.* 1.3 g of the prepared sample immobilized on a glass fiber membrane was put inside the reactor. For PC system, a 300 W Xe lamp (λ > 420 nm with an UV filter, light intensity: 30 mW cm^{-2}, PLS-SXE300/300UV, Beijing Perfectlight Technology Co., Ltd) was used as light source as reported in Ref. [24] (Fig. S2) and a cooler was applied to ensure the system's temperature ≤ 30 °C. For TC system, a plate heater, a digital temperature-indicating regulator and a thermocouple were used to control the temperature ranged from 50 °C to 240 °C inside the reactor. For PTC system, both light and temperature control apparatuses were open. Notably, the light used in this experiment was highly dominated by visible light (420–700 nm) with a small amount of infrared light. Meanwhile, the total intensity of the light herein of 30 mW cm^{-2} was far lower than that in previous work (270.3 mW cm^{-2}), where infrared light contributed to 65.2% and then significantly increased the reaction temperature [14]. Thus, due to very low intensity of total light and negligible amount of detected infrared light as well as efficient cooler system, the influence of infrared light to the variation of temperature in PC and PTC systems could be very limited. The concentrations of styrene were analyzed by a gas chromatography (GC-900A) equipped with a flame ionization detector that samples were collected at regular intervals using a gastight locking syringe (Agilent, Australia), and a 200 μL gas sample was injected into the column for concentration determination in the splitless mode.

3. Results and discussion

3.1. Characterization

The effect of metal ion substituting position A or B of ABO_3 to resulted perovskites' properties is firstly compared. Fig. 1a and b show the XRD patterns of the prepared $ANiO_3$ (A = La, Ce, Sm) and $LaBO_3$ (B = Cr, Mn, Fe, Co, Ni) perovskites, respectively. Clearly, all samples show strong diffraction peaks in the scanning range (10°–80°), indicating high purity and crystallinity of these samples after high temperature treatment. Moreover, their characteristic peaks are all well matched with that of standard perovskite ABO_3 from JCPDS cards as well as previous references [20,25], suggesting the successful synthesis of position A or B substituted
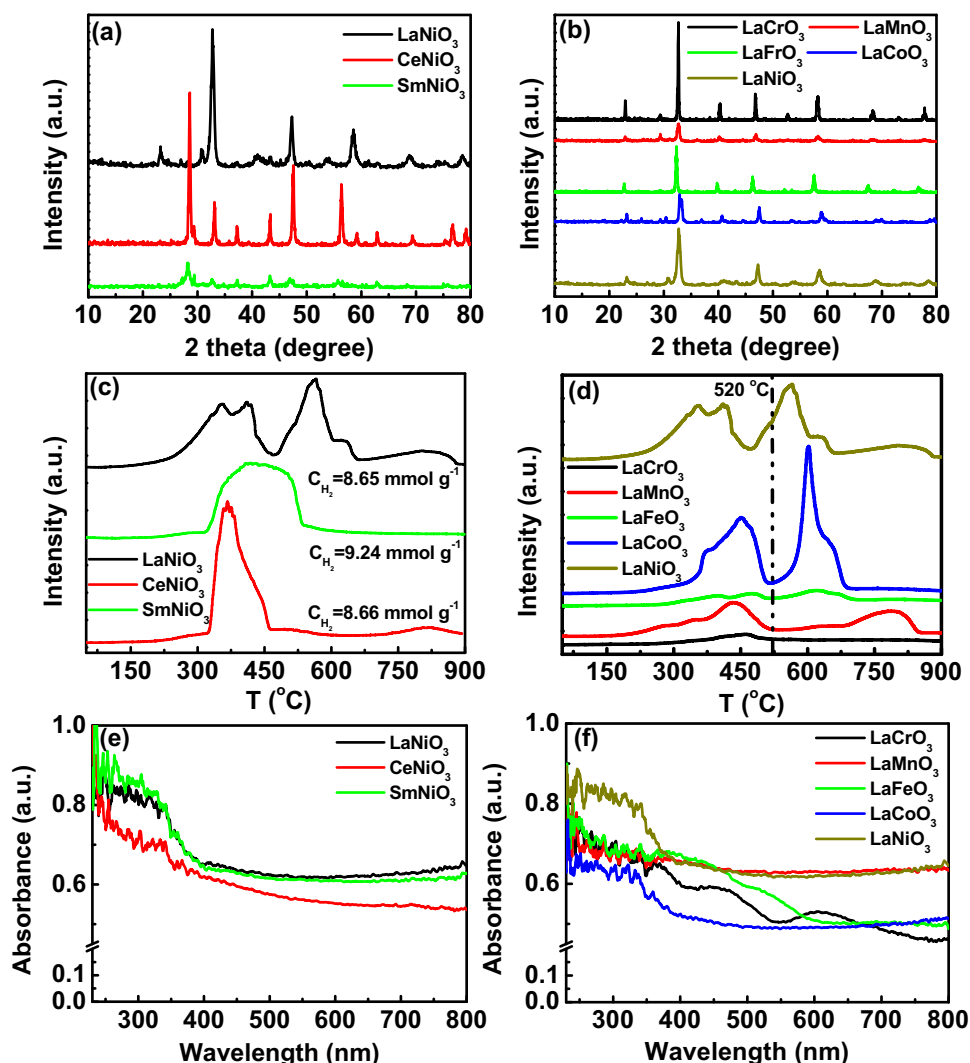
Fig 1. XRD patterns (a, b), UV–vis absorption spectra (c, d) and H_2-TPR curves (e, f) of the prepared ABO_3-type perovskites.

ABO_3 perovskites by using simple soft-templated sol-gel with post-calcination method.

The reducibility of the synthesized perovskites is further compared according to H_2-TPR characterization. In the case of $ANiO_3$ (Fig. 1c), only one reduction peak is found for both $CeNiO_3$ and $SmNiO_3$, contributing to the elimination of adsorbed oxygen and reduction of Ni^{3+} to Ni^{2+} [26]. However, extra reduction region is observed for $LaNiO_3$, ascribing to further reduction of Ni^{2+} to Ni under higher temperature. These results indicate that $LaNiO_3$ may possess higher thermocatalytic reactivity than $CeNiO_3$ and $SmNiO_3$. Meanwhile, these $ANiO_3$ perovskites display very close H_2 consumption amounts of 8.65, 9.24 and 8.66 mmol g^{-1} for $LaNiO_3$, $CeNiO_3$ and $SmNiO_3$, suggesting similar oxidation ability of them. Clearly, these perovskites show negligible enhancement of their oxidizabilities after position A substitution. However, significantly different H_2-TPR curves are obtaiend for position B sutituted $LaBO_3$ perovskites as displayed in Fig. 1d. As shown in the figure, two obvious regions can be observed for $LaCoO_3$, $LaMnO_3$, $LaFeO_3$ and $LaNiO_3$, at low temperature one ($\leq 520\,°C$) and high temperature one ($>520\,°C$), respectively. Similar to $ANiO_3$, the first region is contributed to the removal of the adsorbed oxygen species and the reduction of B^{X+} into $B^{(X-1)+}$ ions, while the second one is ascribed to the further reduction of $B^{(X-1)+}$ to $B^{(X-2)+}$ ions [27]. Notably, only a small peak is observed at around 461 °C for $LaCrO_3$. This is because

that Cr^{3+} ion in $LaCrO_3$ structure is highly stable and hence cannot be reduced under the experimental conditions employed in this work. Similar result has also been reported in the literature [28]. Thus the small peak observed in this profile could be attributed to the adsorbed oxygen or formed La_2CrO_6 during the synthesis of $LaCrO_3$. Since in practical application, the efficiency and degradation rate of organics at low temperature is more important than that at high one, the low-temperature region of H_2-TPR curves are then especially focused in this work. The accumulated H_2 consumption amounts of $LaCoO_3$, $LaMnO_3$, $LaFeO_3$, $LaCrO_3$ and $LaNiO_3$ from room temperature to 520 °C are 7.14, 4.26, 0.90, 1.49 and 4.72 mmol g^{-1}, respectively. Obviously, $LaCoO_3$ shows the highest H_2 consumption amount, followed by $LaNiO_3$, $LaMnO_3$, $LaFeO_3$ and $LaCrO_3$ at the low temperature range, suggesting that more active centers may exist on $LaCoO_3$, $LaNiO_3$ and $LaMnO_3$ surfaces, leading to better oxidation ability and then higher catalytic activity than other perovskites, which is also agreed well with that reported by Shi et al. [29].

The optical properties of the prepared $ANiO_3$ and $LaBO_3$ perovskites are further investigated in detail to compare the effect of position A or B substitution to their light absorption capabilities and hence the photocatalytic enhancement possibility to the catalytic activity of perovskites, since the absorption and capture of light is the initial and key step of photocatalysis. As Fig. 1e and
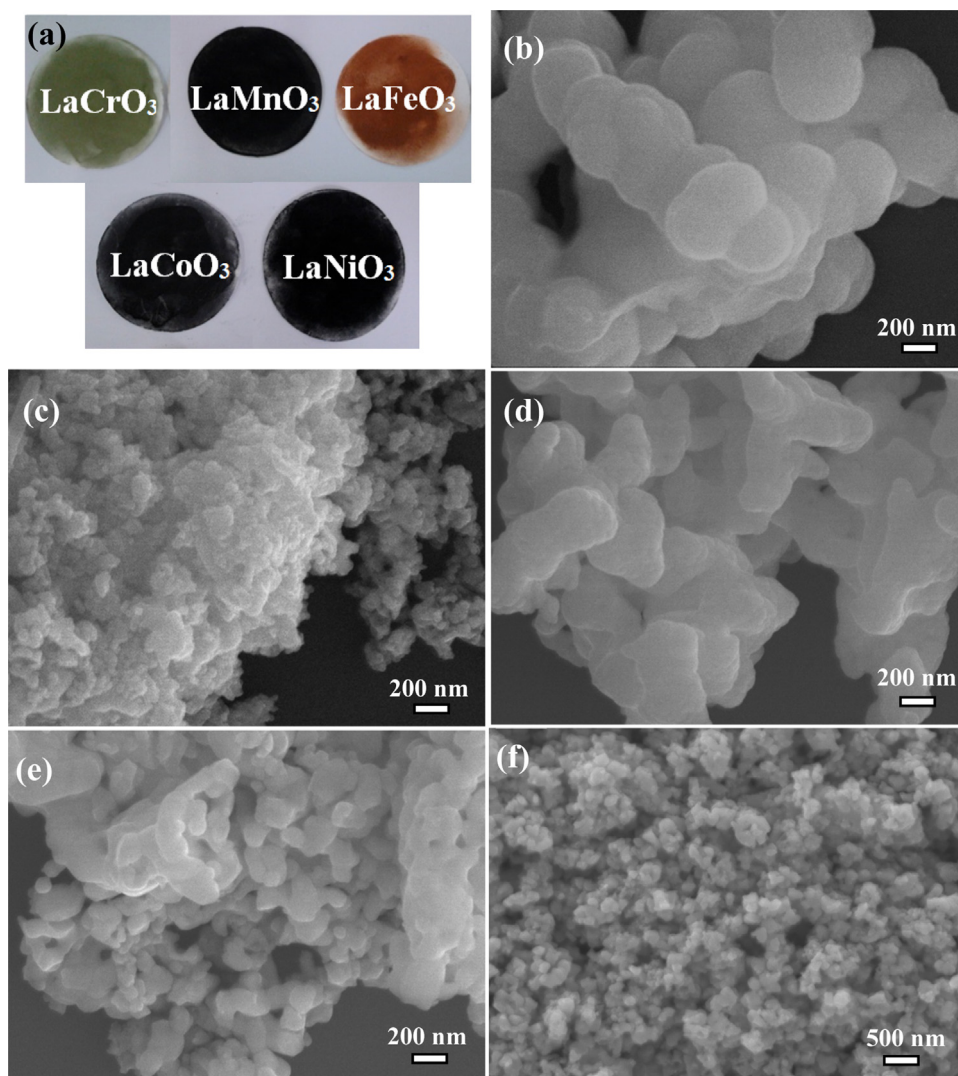
Fig. 2. Photos (a) and SEM images of the prepared $LaBO_3$, (b: $LaCrO_3$, c: $LaMnO_3$, d: $LaFeO_3$, e: $LaCoO_3$, f: $LaNiO_3$).

f show, all synthesized ABO_3-type perovskites show excellent UV and visible light absorption abilities. Further observation reveals that three $ANiO_3$ samples show very similar UV–vis absorption curves and similar visible light absorbance, indicating the possibly same visible-light-driven PC activity and then enhancement to TC. Meanwhile, very close bandgaps (2.4–2.7 eV) are also obtained for $ANiO_3$, again implying their similar visible light response and then PC activity. In contrast, the $LaBO_3$ perovskites display greatly different UV–vis absorption curves, while $LaMnO_3$ and $LaNiO_3$ possess the highest visible light absorbance abilities, probably due to their deep black natures (Fig. 2a). Furthermore, the estimated bandgaps of these perovskites follow the order of $LaCrO_3$ (3.1 eV) > $LaCoO_3$ (2.9 eV) > $LaMnO_3$ (2.5 eV) > $LaNiO_3$ (2.4 eV) > $LaFeO_3$ (2.1 eV). And the narrower bandgap should allow more efficient transfer of photogenerated electron, suppressing the recombination of electron and holes [30]. Thus, sample $LaFeO_3$, $LaNiO_3$ and $LaMnO_3$ may possess the potentially higher visible light photocatalytic activity than $LaCrO_3$ and $LaCoO_3$.

Based on the above results, it can be concluded that ABO_3-type perovskites with positon A substituted by metal ion show much lower enhancement to their oxidative and visible-light-absorption properties in comparison with that position B substitution. This is probably due to that B ion locates at the 3d orbit to constitute the conduction band, while to substitute it with different

metal ion can significantly alter the bandgap and then correspondingly physicochemical properties, such as light response, redox-activity, etc. Similar phenomenon has also been reported in previous research [31]. Thus, $LaBO_3$ perovskites with different position B substituted might show attractive enhancement of PC, TC and PTC performances toward gaseous pollutant degradation, which will be elaborately discussed below.

Besides structural and optical properties, the morphology of prepared perovskite materials might also be influenced after different B ion substitution. Fig. 2b–f display the corresponding SEM images of the prepared $LaBO_3$. As can be seen, all prepared perovskites are consisted of aggregated particles with variable size. Further observation reveals that these particles stack closely to form lamellar and porous structure, which would facilitate the transfer of organics as well as provide larger reaction surfaces and more active sites [32]. Moreover, it can be found that the size of the obtained $LaNiO_3$ and $LaMnO_3$ particle is the smallest, followed by $LaCoO_3$, $LaFeO_3$ and $LaCrO_3$, which is very consistent with the XRD results. And the smallest-sized $LaNiO_3$ and $LaMnO_3$ particles are beneficial for improving the photocatalytic activity due to their large specific areas, which ensures efficient light absorption (Fig. 1f) and provides more reactive sites for the degradation reactions, leading to the higher catalytic activity. Similar result can also be obtained from previous report [33].
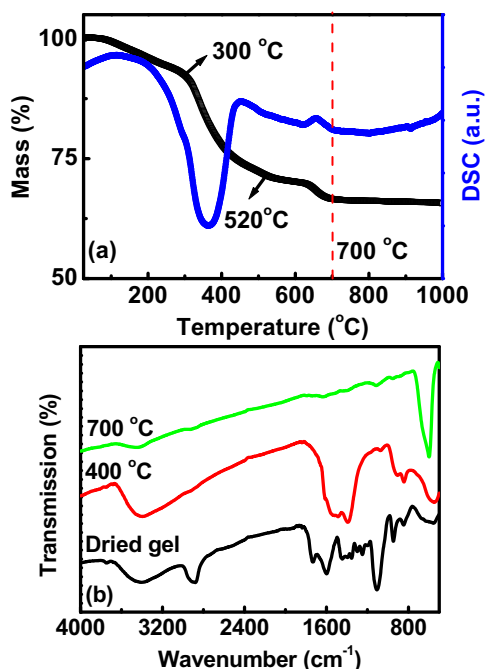
Fig. 3. TG/DSC (a) and FT-IR (b) curves of as-prepared LaCrO₃ gel and after different temperature calcination.

3.2. Formation mechanism of perovskite materials

To understand the formation mechanism of the LaBO₃ perovskites, the TG/DSC curves of as-prepared gel (taking LaCrO₃ as an example) are also conducted and the relative data are shown in Fig. 3a. Clearly, three temperature ranges can be divided during the preparation procedure. The first one is from 100 °C to 300 °C, in which about 8% weight loss is observed, mainly due to the evaporation of H₂O [34]. Second range is from 300 °C to 520 °C with the weight loss of ca. 20%, due to the pyrolysis of PEG linked material [35]. Furthermore, about 6% weight loss is obtained in the range of 520 °C–700 °C, owing to the decomposition of residue organics and intermediates. And no obvious weight loss occurs with increasing the thermal treatment temperature to 1000 °C, indicating that highly thermal stable products can be formed at 700 °C.

Furthermore, the corresponding FT-IR curves are also shown in Fig. 3b. As seen, the dried gel contains a lot of functional groups, including −OH (3399 and 1250 cm⁻¹), −C=O (1730 and 1601 cm⁻¹), C−H (2893 cm⁻¹) and −C−O (833−1106 cm⁻¹), etc. Moreover, a wide peak centered at 549 cm⁻¹ is also observed which is attributed to the complexation of metal ion with template to form metal−O and metal−O−metal bonds [36]. After calcined at 400 °C, most functional groups disappear. However, besides the peak centered at 549 cm⁻¹ with the enhanced intensity, the peaks at 1468 and 843 cm⁻¹ still exist, which are related to the carbonate groups. With further increasing the pyrolysis temperature to 700 °C, these carbonate groups are also removed and another two new peaks centered at around 600 and 400 cm⁻¹ are formed, which are the stretching and bending vibration of BO_6 octahedron in perovskites [37], indicating the formation of perovskite LaCrO₃. Similar results can also be found from FT-IR curves of other prepared LaBO₃ samples (Fig. S3).

Based on above characterization results, a possible complexation-carbonation-oxidation formation mechanism is proposed as follows: during the sol-gel process, the metal ions firstly hydrolyze to form hydroxides, which are then chelated with citric acid to form metal hydroxides-citrate complexes: $La_xB_y(C_6H_8O_7)_z$ [31]. Meanwhile, PEG molecules lose their bond-

ing water during aging process to produce free PEG molecules, which can be easily adsorbed onto the surface of the formed metal hydroxides–citrate complex to generate tightly "metal hydroxides-citrate-PEG" complexes [38]. Moreover, PEG can enhance the growth kinetic of colloids and then eventually produces an anisotropic growth of the perovskites [39]. When thermal treatment is conducted in air under relatively low temperature (≤400 °C), the complexes decompose and carbonate-containing compounds are formed such as $LaBO_{3−X}(CO_3)_x$. With further increasing the temperature, crystalline LaBO₃ (B = Cr, Mn, Fe, Co, Ni) perovskites are obtained after completely oxidizing the carbonate-containing compounds. The use of both citric acid and PEG enables the control synthesis of uniform perovskite with small particles size and porous structures [39].

3.3. Catalytic performance assessment

After discussing the formation process of these LaBO₃-type perovskites, their catalytic activities are further evaluated. Fig. 4 displays the PC, TC and PTC degradation curves of styrene on different perovskites. As Fig. 4a and d show, after visible light illumination for 120 min, about 26.0%, 43.1%, 61.5%, 39.3% and 27.7% of styrene are photocatalytically degraded by LaCrO₃, LaMnO₃, LaFeO₃, LaCoO₃ and LaNiO₃, with the degradation rate constants of 0.0049, 0.0054, 0.0071, 0.0063 and 0.0039 min⁻¹, respectively. Clearly, all prepared perovskites show visible light photocatalytic degradation capabilities to gaseous styrene, while LaFeO₃ possesses the highest one, possibly due to its smallest bandgap and then most efficient transfer of photogenerated electron [40,41]. In comparison with PC, all perovskites show significantly increased TC activities under the reaction temperature of 140 °C that the degradation efficiencies of styrene (the rate constants) by LaCrO₃, LaMnO₃, LaFeO₃, LaCoO₃ and LaNiO₃ are obtained as 70.1%, 92.7%, 85.2%, 92.5% and 97.6% (0.0105, 0.0263, 0.0242, 0.0291 and 0.0341 min⁻¹) within the same degradation period, respectively (Fig. 4b and d). As expected, the order of TC activity of the prepared perovskites is consistent with the H₂-TPR results, confirming that more H₂ consumption leads to higher TC activity. When visible light is introduced into TC system, further enhancement of degradation efficiency and acceleration of degradation rate is both observed for LaCrO₃, LaMnO₃, LaFeO₃ and LaNiO₃. As Fig. 4c shows, after PTC reaction of 40 min, about 42.8%, 96.6%, 82.0% and 80.1% of styrene are degraded by LaCrO₃, LaMnO₃, LaFeO₃ and LaNiO₃, which are by far higher than that in TC system at the same time intervals (31.8%, 68.6%, 67.8% and 76.5%). Meanwhile, the degradation rate constants are accordingly increased from 0.0105, 0.0263, 0.0242 and 0.03411 min⁻¹ to 0.0150, 0.0782, 0.0399 and 0.0391 min⁻¹ (Fig. 4d). Obviously, the PC shows the higher enhancement of TC activity for LaMnO₃ than LaFeO₃, LaCrO₃ and LaNiO₃, probably owing to the synergetic effect of its small crystal size and bandgap as well as high visible light absorption ability and reducibility. Detail enhancement mechanism will be given below. It should be noted that the PTC degradation curve of LaCoO₃ is almost overlapped with TC one, indicating negligible synergetic effect of PC and TC toward styrene degradation onto LaCoO₃ in this study.

Based on above results, it can be found that PC could enhance the TC activity of different LaBO₃ to different extents under a relatively moderate temperature (eg., 140 °C), while raising temperature may further increase the performance. Thus, the effect of temperature on the TC and then PTC activities is investigated, and the corresponding results are shown in Fig. 5 and Figs. S4–S7. As Fig. 5a shows, the TC efficiency of LaMnO₃ toward styrene degradation gradually increases from 71.1% to 100% with increasing the temperature from 50 °C to 240 °C. The corresponding rate constant increases slowly from 0.0165 to 0.0255 min⁻¹ when the temperature raises from 50 °C to 140 °C, which then significantly increases
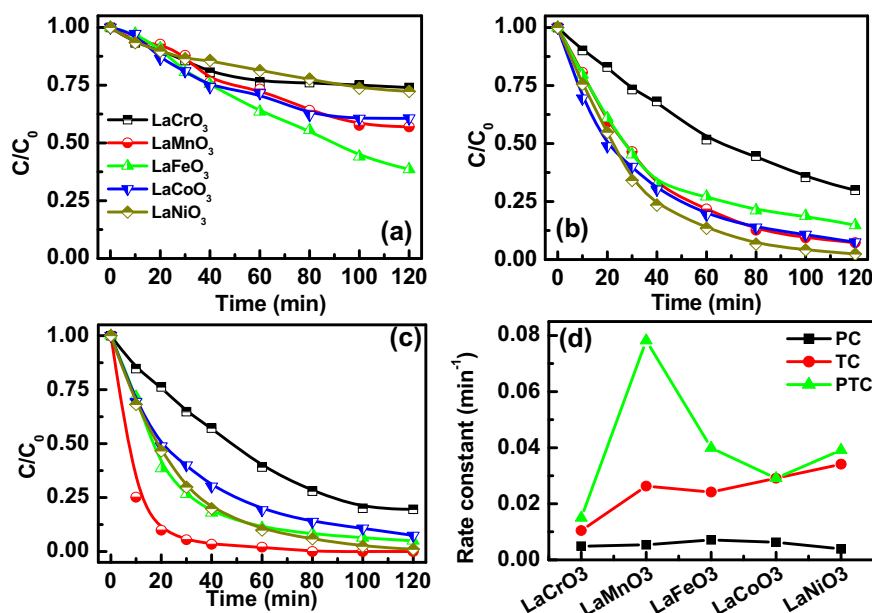
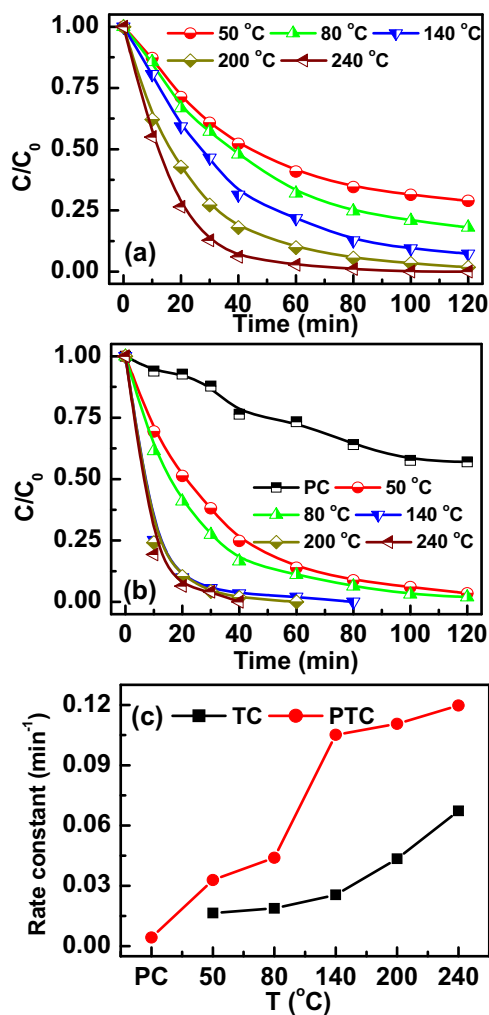**Fig. 4.** PC (a), TC (b), PTC (c) curves and corresponding rate constants (d) of styrene by prepared LaBO$_3$.

Fig. 5. TC (a) and PTC (b) curves as well as corresponding rate constants (c) of styrene by LaMnO$_3$ at different temperatures.

to 0.0435 and 0.0673 min^{-1} with further elevating the temperature to 200 °C and 240 °C, respectively (Fig. 5c). These results indicate that at the relatively high-temperature region (>140 °C), increasing the temperature is more beneficial for the accelerating TC degradation rate of LaMnO$_3$ toward styrene. Similar trend of the removal efficiency and rate constant can also be observed for LaCrO$_3$ and LaFeO$_3$ (Figs. S4–S5). However, for LaCoO$_3$ and LaNiO$_3$, almost linearly increased rate constant are obtained from 0.0158 and 0.0144 min^{-1} to 0.0354 and 0.0380 min^{-1} at the investigated temperature region (50 °C–240 °C) (Figs. S6–S7). To further understand the exact enhancement degree of temperature to the TC rate constant of LaBO$_3$, the ratio of rate constant between 240 °C and 50 °C is calculated, which follows the order of LaFeO$_3$ (5.7) > LaMnO$_3$ (4.1) > LaCrO$_3$ (3.1) > LaNiO$_3$ (2.6) > LaCoO$_3$ (2.2). Meanwhile, LaFeO$_3$ (0.0737 min^{-1}) and LaMnO$_3$ (0.0673 min^{-1}) displayed the highest rate constant at 240 °C. All these results suggest that the increase of reaction temperature will accelerate the TC degradation rate of the prepared perovskites to styrene to different extents, while LaFeO$_3$ shows the highest enhancement performance, probably owing to its narrowest bandgap.

For PTC system, the increase of the temperature from room temperature (PC) to 50 °C results in the sharply enhancement of degradation efficiency (from 43.1% to 96.5%) as well as the rate constant from 0.0043 to 0.0329 min^{-1} for LaMnO$_3$ (Fig. 5b and c), again confirming the significantly enhanced activity after the combination of PC with TC. When further increasing the temperature to 80 °C, slight increase of removal efficiency and rate constant to 98.1% and 0.0440 min^{-1} is observed, indicating the similar contribution of PC to TC activity at the temperature ranged from 50 °C to 80 °C. However, the rate constant (0.1051 min^{-1}) becomes more than twice higher than that at 80 °C with completely degradation of styrene when the temperature reaches 140 °C, which then gradually increases to 0.1106 and 0.1197 min^{-1} as further increasing the temperature to 200 °C and 240 °C, revealing that the enhancement of TC activity of LaMnO$_3$ by PC almost reaches equilibrium when the temperature is set as 140 °C. Interestingly, further comparison of PTC and TC degradation rate constants displays that the degradation rate (0.0440 min^{-1}) of PTC at 80 °C is similar to that of TC at 200 °C (0.0435 min^{-1}), indicating that the addition of PC into TC system can efficiently decrease the temperature that needed to achieve
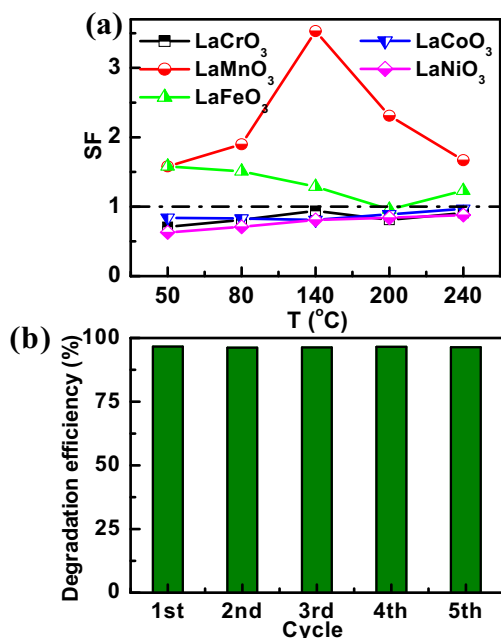
Fig. 6. (a) SF of the prepared perovskites at different temperatures and (b) the stability test of PTC degradation efficiency of styrene by LaMnO₃.

high degradation activity toward styrene herein. Similar results can also be obtained for other perovskites with different enhancement characteristics (Figs. S4–S7), possibly owing to different synergetic effect between PC and TC of these perovskites.

To intuitively figure out the synergetic effect of PC and TC in the PTC system, synergistic factor (SF) is used [42,43], which stands for the ratio between PTC rate constant and total rate constants of PC with TC. If SF > 1, there is synergetic effect between PC and TC. Conversely, synergistic effect is not obvious [44]. The SFs of the prepared perovskites at different reaction temperature are calculated and shown in Fig. 6a. As seen, the SF values of LaCrO₃ (from 0.71 to 0.94), LaCoO₃ (from 0.81 to 0.97) and LaNiO₃ (from 0.63 to 0.88)

are all less than 1, indicating the negligible promotion of TC activity by PC for these three perovskites in the studied temperature range of 50–240 °C. However, high SF value is observed for LaFeO₃ at 50 °C (1.58), which slightly decreases to 1.23 at 240 °C, suggesting PC can somewhat enhance the TC degradation activity toward styrene for LaFeO₃, leading to higher PTC efficiency. Interestingly, same SF value is obtained for LaMnO₃ at 50 °C (1.58), indicating same PTC synergetic effect of LaFeO₃ and LaMnO₃ at relatively low temperature. However, the SF value of LaMnO₃ then significantly increases and peaks at 3.53 (140 °C), which then decreases to 1.67 with the further increase of the temperature to 240 °C, revealing that too high temperature is not beneficial for the improvement of synergetic effect of PC and TC, and the highest synergetic effect of PC and TC for LaMnO₃ can be obtained under the temperature of 140 °C. This may be because that too high temperature will lower the active energy of styrene oxidation as well as lead to dissociation of H₂O onto the surface of perovskites and then weaken the OH-initiated oxidation of styrene, which is also agreed with other research works [12,45]. More importantly, LaMnO₃ shows the highest SF value among the prepared perovskites, probably ascribing to the synergetic effect of its crystal size and bandgap as well as visible light absorption ability and reducibility. Besides the activity, the combination of PC and TC can also improve the stability of the prepared perovskite catalysts. As Fig. 6b shows, after five continuous degradation cycles of styrene onto LaMnO₃ within 40 min, PTC system of LaMnO₃ can also effectively maintain the activity with almost the same removal efficiency (ca. 96.6%) to styrene. All these results indicate that the combination of PC with TC technologies over the perovskite catalysts can provide an efficient and practical way to utilize the total energy from both light and heat for the remediation of atmospheric environment pollutions.

3.4. Photothermocatalytic mechanism clarification

Previous report has confirmed that catalytic oxidation of VOCs on metal oxide follows the Mars-van Krevelen redox cycle, where VOCs is firstly oxidized by the lattice oxygen of catalyst, while the reduced oxide catalyst is re-oxidized later by gaseous oxygen [13]. Moreover, the more active hole-trapped lattice oxygen ion in the
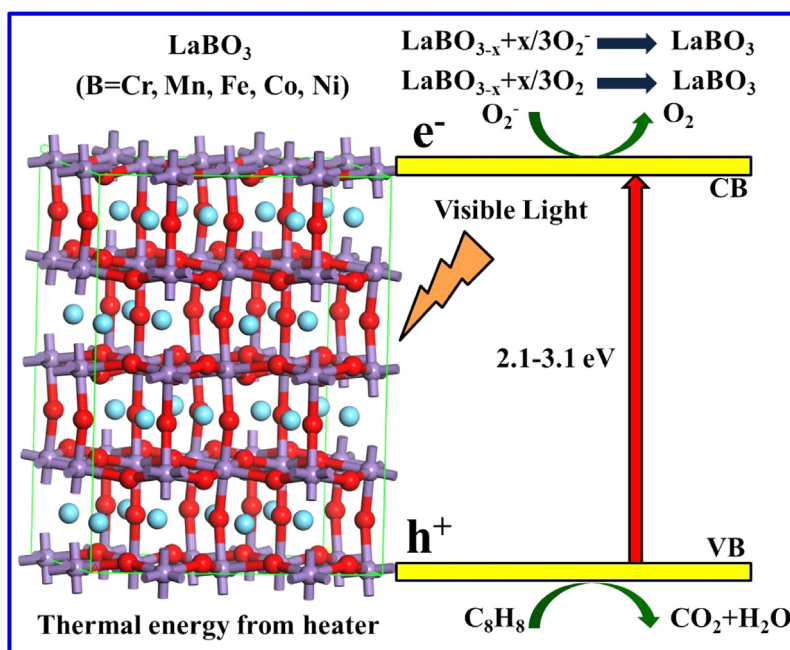

Fig. 7. Photothermocatalytic degradation mechanism of styrene on LaBO₃ perovskite by the combination of visible photons with thermal energy from a heater.

oxide catalyst will be generated under visible light irradiation [11]. Meanwhile, increasing temperature will enhance the mobility of lattice oxygen ion [46]. Thus in this study, as shown in the H$_2$-TPR results, B ion in LaBO$_3$ is more easily reduced from B^{X+} into B$^{(X-1)+}$ ions to form LaBO$_{3-x}$, which is then re-oxidized just by gaseous oxygen in TC system on perovskite at low temperature. While for PTC process, besides of gaseous oxygen, active oxygen species such as O^{2-} could also be generated from the reduction of oxygen by photogenerated electrons in perovskite conduction band under visible light irradiation. Hence, both gaseous oxygen and formed active oxygen species re-oxidize the reduced perovskite (LaBO$_{3-x}$) to form LaBO$_3$ (Fig. 7). More importantly, much higher synergetic PTC efficiency can be obtained than a combination of the alone PC and TC efficiency, because that more active lattice oxygen of the perovskite can be induced under visible light irradiation which then accelerates the above redox cycle of LaBO$_3$/LaBO$_{3-x}$. In addition, higher reaction temperature leads to more efficient suppress of the recombination of photogenerated holes and electrons, resulting in enhanced PTC efficiency with increasing temperature.

Notably, different enhancement extent of PTC efficiency is obtained for LaBO$_3$ with different B ion substitution, while LaMnO$_3$ apparently shows the best PTC activity for gaseous styrene in this study. This significantly enhanced PTC activity may be attributed to the synergistic effects of several factors such as crystal size, bandgap, visible light response and redox property of this perovskite. According to previous report [5], to realize high PTC efficiency, the photocatalyst must satisfy two requirements at the same time: strong light adsorption and highly efficient thermocatalytic activity. In this study, potentially abundant catalytic reaction sites and then high PC, TC and PTC catalytic activity for degradation reactions can be obtained due to the small crystal size (ca. 16.6 nm) of LaMnO$_3$ [47]. Meanwhile, it displays relatively narrow bandgap (2.5 eV) among the prepared perovskites, resulting in the highly efficient visible light absorption (seen from UV–vis curve in Fig. 1f). Besides, LaMnO$_3$ also shows very high reducibility at low temperature region (seen from H$_2$-TPR curve in Fig. 1d), suggesting high oxidation ability as well as fast redox cycle of LaMnO$_3$/LaMnO$_{3-x}$. This is because that low-temperature reducibility is one of the critical factors for the oxidation reaction [48]. Therefore, the significant enhancement of PTC efficiency of LaMnO$_3$ toward styrene degradation is attributed to synergetic effect of its very good PC and TC activities from small crystal size and narrow bandgap as well as high visible light absorption ability and reducibility.

4. Conclusions

In summary, ABO$_3$ (A = La, Ce, Sm; B = Cr, Mn, Fe, Co, Ni) perovskites have been simply synthesized via a sol-gel-calcination method through a complexation-carbonation-oxidation process. In comparison with limited effect on the properties of ANiO$_3$ after position A substitution, the prepared position B substituted LaBO$_3$ (B = Cr, Mn, Fe, Co, Ni) perovskites exhibited significantly enhanced thermocatalytic activity and stability for gaseous styrene degradation under the visible light irradiation, due to the synergetic effect of their very good photocatalytic and thermocatalytic activities from small crystal size and narrow bandgap as well as high visible light absorption ability and reducibility. This novel strategy using the synergetic effect between the visible-light-driven photocatalysis and temperature-induced thermocatalysis of perovskite catalyst is applicable to develop other efficient catalysts for the atmospheric environment purification using light and heat energy together.

Appendix A. Supplementary data

Supplementary data associated with this article can be found, in the online version, at http://dx.doi.org/10.1016/j.apcatb.2017. 02.066.

References

[1] C.M. Nunez, G.H. Ramsey, E.J. Kong, M.A. Bahner, R.S. Wright, C.A. Clayton, J.N. Baskir, J. Air Waste Manag. Assoc. 49 (1999) 256–267.
[2] T.C. An, Y. Huang, G.Y. Li, Z.G. He, J.Y. Chen, C.S. Zhang, Environ. Int. 73 (2014) 186–194.
[3] M.S. Kim, G. Liu, H.K. Cho, B.W. Kim, J. Hazard. Mater. 190 (2011) 537–543.
[4] V. Blasin-Aube, J. Belkouch, L. Monceaux, Appl. Catal. B: Environ. 43 (2003) 175–186.
[5] H.H. Liu, Y.Z. Li, Y. Yang, M.Y. Mao, M. Zeng, L. Lan, L. Yun, X.J. Zhao, J. Mater. Chem. A 4 (2016) 9890–9899.
[6] W.Y. Jung, Y.I. Song, K.T. Lim, G.D. Lee, M.S. Lee, S.S. Hong, J. Nanosci. Nanotechnol. 15 (2015) 652–655.
[7] W.Y. Jung, K.T. Lim, G.D. Lee, M.S. Lee, S.S. Hong, J. Nanosci. Nanotechnol. 13 (2013) 6120–6124.
[8] C.H. Zhang, Y.L. Guo, Y. Guo, G.Z. Lu, A. Boreave, L. Retailleau, A. Baylet, A. Giroir-Fendler, Appl. Catal. B: Environ. 148 (2014) 490–498.
[9] J.M. Giraudon, A. Elhachimi, F. Wyrwalski, S. Siffert, A. Aboukais, J.F. Lamonier, G. Leclercq, Appl. Catal. B: Environ. 75 (2007) 157–166.
[10] M.J. Suh, Y.K. Park, S.K. Ihm, Catal. Today 265 (2016) 210–217.
[11] Y.Z. Li, Q. Sun, M. Kong, W.Q. Shi, J.C. Huang, J.W. Tang, X.J. Zhao, J. Phys. Chem. C 115 (2011) 14050–14057.
[12] X.X. Wang, D.W. Zeng, C.S. Xie, Mater. Lett. 139 (2015) 336–339.
[13] Y.Z. Li, J.C. Huang, T. Peng, J. Xu, X.J. Zhao, ChemCatChem 2 (2010) 1082–1087.
[14] M.Y. Mao, Y.Z. Li, J.T. Hou, M. Zeng, X.J. Zhao, Appl. Catal. B: Environ. 174 (2015) 496–503.
[15] Y.L. Zheng, W.Z. Wang, D. Jiang, L. Zhang, Chem. Eng. J. 284 (2016) 21–27.
[16] M. Zeng, Y.Z. Li, M.Y. Mao, J.L. Bai, L. Ren, X.J. Zhao, ACS Catal. 5 (2015) 3278–3286.
[17] E. Grabowska, Appl. Catal. B: Environ. 186 (2016) 97–126.
[18] P. Kanhere, Z. Chen, Molecules 19 (2014) 19995–20022.
[19] C.X. Qin, Z.Y. Li, G.Q. Chen, Y. Zhao, T. Lin, J. Power Sources 285 (2015) 178–184.
[20] K. Peng, L.J. Fu, H.M. Yang, J. Ouyang, Sci. Rep. U. K. 6 (2016).
[21] R.S. Hu, C. Li, X. Wang, Y. Sun, H.X. Jia, H.Q. Su, Y.L. Zhang, Catal. Commun. 29 (2012) 35–39.
[22] M. Humayun, Z.J. Li, L.Q. Sun, X.L. Zhang, F. Raziq, A. Zada, Y. Qu, L.Q. Jing, Nanomaterials-Basel 6 (2016).
[23] J.J. Ding, J. Bao, S.N. Sun, Z.L. Luo, C. Gao, J. Comb. Chem. 11 (2009) 523–526.
[24] G.Y. Li, X. Nie, J.Y. Chen, Q. Jiang, T.C. An, P.K. Wong, H.M. Zhang, H.J. Zhao, H. Yamashita, Water Res. 86 (2015) 17–24.
[25] Y. Yamada, K. Yano, D.C. Hong, S. Fukuzumi, Phys. Chem. Chem. Phys. 14 (2012) 5753–5760.
[26] Y.C. Wei, Z. Zhao, J.Q. Jiao, J. Liu, A.J. Duan, G.Y. Jiang, Catal. Today 245 (2015) 37–45.
[27] B.Z. Gao, J.G. Deng, Y.X. Liu, Z.X. Zhao, X.W. Li, Y. Wang, H.X. Dai, Chin. J. Catal. 34 (2013) 2223–2229.
[28] M.C. Alvarez-Galvan, V.A.D. O'Shea, G. Arzamendi, B. Pawelec, L.M. Gandia, J.L.G. Fierro, Appl. Catal. B: Environ. 92 (2009) 445–453.
[29] H.X. Shi, J.Y. Chen, G.Y. Li, X. Nie, H.J. Zhao, P.K. Wong, T.C. An, ACS Appl. Mater. Interfaces 5 (2013) 6959–6967.
[30] J.S. Lee, K.H. You, C.B. Park, Adv. Mater. 24 (2012) 1084–1088.
[31] S. Thirumalairajan, K. Girija, I. Ganesh, D. Mangalaraj, C. Viswanathan, A. Balamurugan, N. Ponpandian, Chem. Eng. J. 209 (2012) 420–428.
[32] J.Y. Chen, X.L. Liu, G.Y. Li, X. Nie, T.C. An, S.Q. Zhang, H.J. Zhao, Catal. Today 164 (2011) 364–369.
[33] T.C. An, J.Y. Chen, X. Nie, G.Y. Li, H.M. Zhang, X.L. Liu, H.J. Zhao, ACS Appl. Mater. Interfaces 4 (2012) 5988–5996.
[34] W.H. Liu, S.L. He, Y. Wang, Y. Dou, D.J. Pan, Y. Feng, G. Qian, J.Z. Xu, S.D. Miao, Electrochim. Acta 144 (2014) 119–126.
[35] A.P. Su, Y. Zhou, Y.H. Yao, C.M. Yang, H. Du, Microporous Mesoporous Mater. 159 (2012) 36–41.
[36] N. Arconada, Y. Castro, A. Duran, Appl. Catal. A: Gen. 385 (2010) 101–107.
[37] N.A. Merino, B.P. Barbero, P. Grange, L.E. Cadus, J. Catal. 231 (2005) 232–244.
[38] T.C. An, J.K. Liu, G.Y. Li, S.Q. Zhang, H.J. Zhao, X.Y. Zeng, G.Y. Sheng, J.M. Fu, Appl. Catal. A: Gen. 350 (2008) 237–243.

[39] I.A. Abdel-Latif, A.A. Ismail, H. Bouzid, A. Al-Hajry, J. Magn. Magn. Mater. 393 (2015) 233–238.

[40] J.Y. Chen, H.M. Zhang, P.R. Liu, Y.B. Li, X.L. Liu, G.Y. Li, P.K. Wong, T.C. An, H.J. Zhao, Appl. Catal. B: Environ. 168 (2015) 266–273.

[41] Y.B. Li, H.M. Zhang, P.R. Liu, D. Wang, Y. Li, H.J. Zhao, Small 9 (2013) 3336–3344.

[42] R.A. Torres, J.I. Nieto, E. Combet, C. Petrier, C. Pulgarin, Appl. Catal. B: Environ. 80 (2008) 168–175.

[43] R.A. Torres-Palma, J.I. Nieto, E. Combet, C. Petrier, C. Pulgarin, Water Res. 44 (2010) 2245–2252.

[44] T.C. An, Y. Xiong, G.Y. Li, C.H. Zha, X.H. Zhu, J. Photochem. Photobiol. A: Chem. 152 (2002) 155–165.

[45] X.Z. Fu, L.A. Clark, W.A. Zeltner, M.A. Anderson, J. Photochem. Photobiol. A: Chem. 97 (1996) 181–186.

[46] X.W. Liu, K.B. Zhou, L. Wang, B.Y. Wang, Y.D. Li, J. Am. Chem. Soc. 131 (2009) 3140–3141.

[47] Y.J. Xu, Y.B. Zhuang, X.Z. Fu, J. Phys. Chem. C 114 (2010) 2669–2676.

[48] Y.L. Zheng, W.Z. Wang, D. Jiang, L. Zhang, X.M. Li, Z. Wang, Phys. Chem. Chem. Phys. 18 (2016) 18180–18186.